Plasma Chemistry and Plasma Processing, Vol. 21, No. 4, December 2001 (© 2001)

Determination of the Nitrogen Atom Density in the Afterglow of a Nitrogen and Helium, Nonequilibrium, Atmospheric Pressure Plasma

S. E. Babayan,[1] G. Ding,[1] and R. F. Hicks[1,2]

Received October 12, 2000; accepted January 24, 2001

Three methods have been examined for evaluating the concentration of nitrogen atoms in the afterglow of a nonequilibrium, helium-stabilized, atmospheric pressure plasma. These are nitric oxide titration, absolute emission intensity of $N_2(B\,^3\Pi_g)$ and temporal decay of the $N_2(B\,^3\Pi_g)$ emission. To employ the second method, the rate constants for the recombination of N atoms into $N_2(B\,^3\Pi_g)$, at different vibrational levels of the B state, were determined. The third newly developed method has three advantages over the other two techniques: (1) it can predict the N-atom density for the entire afterglow, (2) it does not require calibration of the $N_2(B\,^3\Pi_g)$ emission intensity, and (3) it does not disturb the gas flow. According to these measurements, the atmospheric pressure plasma produced a high density of nitrogen atoms, exceeding $4.0 \times 10^{15}\,cm^{-3}$ at the edge of the discharge for 10 Torr N_2 in 745 Torr He at 375 K and 15.5 W/cm^3.

KEY WORDS: Nitrogen atoms; nitrogen plasma; atmospheric pressure plasma.

1. INTRODUCTION

Nitrogen plasmas have been studied for many years, because these discharges create a high density of N atoms that may be used for materials processing, such as in the deposition of silicon nitride films.[1–9] Furthermore, there is interest in nitrogen plasmas that operate at atmospheric pressure, since they offer several advantages over their low-pressure counterparts. A stable, low-temperature, atmospheric pressure plasma opens up a new processing window. This variation in pressure by a factor of 100 may give rise to alternative chemistry, yielding higher reaction rates or better selectivities to desired products. In addition, large-area substrates, such as those

[1]Department of Chemical Engineering, University of California, Los Angeles, California 90095.
[2]To whom all correspondence should be addressed. e-mail: rhicks@ucla.edu

0272-4324/01/1200-0505$19.50/0

used to make flat panel displays, can be processed more easily without vacuum equipment. Recently, we have developed a plasma source that operates at atmospheric pressure and neutral temperatures below 420 K.[10–14] This stable, homogeneous, arc-less gas discharge can generate a high flux of nitrogen atoms for downstream materials processing, and consequently, is the subject of the present study.

Ground state nitrogen atoms, N(^{4}S), are regarded as the major energy-carrying component in the afterglow of nitrogen plasmas.[15] However, diagnosing nitrogen atoms is a challenging task. Early studies of emission spectra provided no evidence for the presence of this species in the afterglow region.[16] Later, electron spin resonance, mass spectroscopy, and vacuum ultraviolet absorption spectroscopy offered overwhelming evidence for significant concentrations of nitrogen atoms downstream of the discharge. Currently, gas-phase titration is the most widely used method for measuring the absolute density of N atoms.[17–21] However, this method requires a complex experimental setup, and it disrupts the plasma process.

Another way to obtain the nitrogen-atom concentration is to measure the absolute intensity of the first-positive emission spectrum of molecular nitrogen, $N_2(B\,^3\Pi_g)$.[22–25] This technique applies to the late afterglow, where the excited molecule is produced primarily by the recombination of N atoms.[3] However, for high-pressure plasmas, this approach must be modified to include collisional quenching and a shift in the vibrational distribution of excited N_2 molecules.

Although the above techniques can be used to determine the concentration of nitrogen atoms, there is still a need for a simple optical method that does not disrupt the process, is applicable to the entire afterglow, and does not require absolute calibration of the $N_2(B)$ emission intensity. In this manuscript, we propose a method that satisfies these criteria. It is based upon the measurement of the temporal decay rate of the first-positive emission, $N_2(B) \rightarrow N_2(A) + h\nu$. We expect that this approach may find broad application in diagnosing the downstream region of high-pressure nitrogen plasmas.

2. THEORY

2.1. Early and Late Afterglow Regions

As shown in Table I, the afterglow of the nitrogen discharge may be divided into two regions. In the "early" afterglow, the concentration of $N_2(B)$ is governed by the presence of N atoms, $N_2(A)$, and $N_2(C)$ as outlined in reactions (1) to (7). The vibrational levels of B and A states, v' and v'',

Table I. Reaction Mechanism for the Neutral Species in a Nitrogen/Helium Atmospheric-Pressure Plasma

Important reactions	Equation
Early Afterglow	
$N + N + M \xrightarrow{k_1(v',M)} N_2(B\,^3\Pi_g, v') + M$	(1)
$N_2(B\,^3\Pi_g, v') \xrightarrow{k_2(v',v'')} N_2(A\,^3\Sigma_u, v'') + h\nu$	(2)
$N_2(B\,^3\Pi_g, v') + M \xrightarrow{k_3(v',M)} N_2(\neq B) + M$	(3)
$N_2(C\,^3\Pi_u) \longrightarrow N_2(B\,^3\Pi_g) + h\nu$	(4)
$N_2(A\,^3\Sigma_u) + N_2(A\,^3\Sigma_u) \longrightarrow N_2(B\,^3\Pi_g) + N_2$	(5)
$N_2(A\,^3\Sigma_u) + N_2(X, v \geq 6) \longrightarrow N_2(B\,^3\Pi_g) + N_2$	(6)
$N_2(A\,^3\Sigma_u) + N \longrightarrow N_2 + N$	(7)
Late Afterglow	
$N + N + M \xrightarrow{k_1(v',M)} N_2(B\,^3\Pi_g, v') + M$	(1)
$N_2(B\,^3\Pi_g, v') \xrightarrow{k_2(v',v'')} N_2(A\,^3\Sigma_u, v'') + h\nu$	(2)
$N_2(B\,^3\Pi_g, v') + M \xrightarrow{k_3(v',M)} N_2(\neq B) + M$	(3)

M = third body = He in this work.

are indicated in Eqs. (1) and (2), because the rate constants for these reactions depend on the level. The $N_2(C)$ species exhibit a short radiative lifetime of 4.0 μs and are rapidly lost through Eq. (4). On the other hand, the metastable $N_2(A)$ molecules do not undergo radiative decay, but instead are consumed by Eqs. (5) to (7). Alternatively, in the "late" afterglow, the $N_2(A)$and $N_2(C)$ species are present in very low concentrations, so that the mechanism is dominated by the recombination of N atoms and the first positive emission. The techniques described below have been performed in the late afterglow where the reaction chemistry is greatly simplified.

2.2. NO Titration

Nitric oxide titration has been employed by several researchers to determine the density of nitrogen atoms downstream of a plasma.[17–21] The reaction mechanism for N and NO in the late afterglow is presented in Table II.[26,27] At low nitric oxide flow rates ([NO] < [N]), a small amount of oxygen atoms are produced by reaction (8). These oxygen atoms react with nitrogen atoms to produce excited-state NO(B) by reaction (9), which can

Table II. Reaction Mechanism for Nitric Oxide Titration

Reactions	Equation
Low NO Flow rates	
$N + NO \xrightarrow{k_8} N_2 + O$	(8)
$N + O + M \xrightarrow{k_9} NO(B\,^2\Pi) + M$	(9)
$NO(B\,^2\Pi) \xrightarrow{k_{10}} NO + h\nu$	(10)
$NO(B\,^2\Pi) + M \xrightarrow{k_{11}} NO + M$	(11)
$NO + N_2(A\,^3\Sigma_u) \xrightarrow{k_{12}} NO(A\,^2\Sigma) + N_2$	(12)
$NO(A\,^2\Sigma) \xrightarrow{k_{13}} NO + h\nu$	(13)
$NO(A\,^2\Sigma) + M \xrightarrow{k_{14}} NO + M$	(14)
High NO flow rates	
$O + NO + M \xrightarrow{k_{15}} NO_2(A\,^2B_1) + M$	(15)
$NO_2(A\,^2B_1) \xrightarrow{k_{16}} NO_2 + h\nu$	(16)
$NO_2(A\,^2B_1) + M \xrightarrow{k_{17}} NO_2 + M$	(17)

M = third body = He in this work.

return to the ground state either by radiative decay, Eq. (10), or by collisional quenching, Eq. (11). Nitric oxide also reacts with $N_2(A)$ to produce $NO(A)$ by Eq. (12). However, this reaction is only significant when the $N_2(A)$ concentration is close to the nitrogen atom concentration, as in the early afterglow. Nitric oxide is converted from the A state into the ground state by reactions (13) and (14). At high nitric oxide flow rates ([NO] > [N]), the O atoms react with NO by Eq. (15) to produce excited $NO_2(A)$. This species undergoes radiative loss by Eq. (16), or collisional quenching by Eq. (17), producing ground-state NO_2.

According to the mechanism presented in Table II, the $NO(B)$ emission decreases with increasing nitric oxide concentration with [NO] < [N]. This is due to the competition between reactions (9) and (15) for the oxygen atoms. The extinction of this emission corresponds to the titration point, where the N and NO concentrations equal each other. Raising the nitric oxide concentration beyond this point results in an increase in the $NO_2(A)$ and ground-state NO_2 concentrations.

2.3. Absolute Emission Intensity of $N_2(B)$

Noxon[25] first demonstrated that the density of nitrogen atoms can be determined by monitoring the absolute intensity of the first positive band in low pressure plasmas. In the late afterglow, $N_2(B)$ is created and consumed by reactions (1) and (2) in Table I. The absolute emission intensity from the first positive emission, Eq. (2), together with the rate constants k_1 and k_2, can be used to calculate the concentration of N atoms from a material balance on the system. The rate constants have been measured by Campbell[22] and Young *et al.*[23]

To apply this technique at atmospheric pressure, one must account for collisional quenching and the vibrational distribution of $N_2(B)$ states. The latter property depends upon the gas pressure and composition.[28,29] Several authors have studied the vibrational distribution of $N_2(B)$ molecules produced in nitrogen and argon plasmas.[18–30] However, to our knowledge, there has been no report of the reaction rates for recombination of N atoms into $N_2(B, v')$ at each vibrational level, v', in helium at atmospheric pressure. The overall rate and the rates for v' equal to 9, 10, 11, and 12 have been determined in helium at low pressures only.[22–24]

In the late afterglow, $N_2(B, v')$ is produced by reaction (1). Collisional quenching of $N_2(B, v')$ produces nitrogen at states other than $N_2(B, v')$ as indicated in reaction (3). Applying the pseudo-steady-state approximation to $N_2(B)$, one obtains

$$R_1 = R_2 + R_3 \tag{18}$$

where R_1, R_2, and R_3 are the rates of reactions (1) through (3). This expression may be rearranged to solve for the density of $N_2(B, v')$ at a given vibrational level:

$$[N_2(B, v')] = \frac{k_1(v', \mathrm{He})[N]^2[\mathrm{He}]}{\sum_{v''} k_2(v', v'') + k_3(v', N_2)[N_2] + k_3(v', \mathrm{He})[\mathrm{He}]} \tag{19}$$

In Eq. (19), the rate constant k_2 is summed over all vibrational levels, v'', of the A state. At atmospheric pressure and 350 K, the rate constants for reaction (2) are less than $10^5\ s^{-1}$,[31] the nitrogen quenching rate constants, $k_3(v', N_2)$, are approximately $10^{-11}\ cm^3/s$ for each vibrational state,[32] and the helium quenching rate constants, $k_3(v', \mathrm{He})$, are about $10^{-12}\ cm^3/s$ for each vibrational state.[24] The concentrations of nitrogen and helium fed to the plasma were 2.8×10^{17} and $2.1 \times 10^{19}\ cm^{-3}$, respectively. Based on these data, the helium term in the denominator of Eq. (19) is much larger than

the other terms. Therefore, Eq. (19) may be simplified to:

$$[N_2(B, v')] \approx \frac{k_1(v', \mathrm{He})}{k_3(v', \mathrm{He})}[\mathrm{N}]^2 \tag{20}$$

This equation is valid for high pressures only. Inspection of Eq. (20) reveals that the $N_2(B)$ concentration is about 8 orders of magnitude lower than the N atom concentration, and justifies the use of the steady-state approximation above.

The intensity of the $N_2(B)$ emission is related to its concentration by

$$I_{N_2(B)} = k_{\mathrm{inst}} A(v')[N_2(B, v')] \tag{21}$$

where k_{inst} is an instrument calibration constant and $A(v')$ is the Einstein coefficient for the radiative transition. Combining Eqs. (20) and (21), $I_{N_2(B)}$ is related to the nitrogen atom concentration as follows,

$$I_{N_2(B)} = \frac{k_{\mathrm{inst}} A(v') k_1(v', \mathrm{He})}{k_3(v', \mathrm{He})}[\mathrm{N}]^2 = \alpha[\mathrm{N}]^2 \tag{22}$$

where α is a constant. From Eq. (22), $k_1(v', \mathrm{He})$ can be obtained if $I_{N_2(B)}$ [N], and the remaining constants are known. Conversely, once the rate constants, $k_1(v', \mathrm{He})$ and $k_3(v', \mathrm{He})$, and the absolute $N_2(B)$ emission intensity are known, the density of nitrogen atoms may be calculated.

2.4. $N_2(B)$ Temporal Decay

Equation (22) can be modified to be independent of α by taking the natural logarithm of both sides, and then differentiating the resultant equation with respect to time,

$$\frac{d\ln(I_{N_2(B)})}{dt} = \frac{d\ln([\mathrm{N}]^2)}{dt} = \frac{2}{[\mathrm{N}]}\frac{d[\mathrm{N}]}{dt}. \tag{23}$$

In the late afterglow, the nitrogen atoms recombine to form $N_2(B)$ by reaction (1). Thus, $d[\mathrm{N}]/dt$ is given by

$$\frac{d[\mathrm{N}]}{dt} = -2R_1 = -2k_1(v', \mathrm{He})[\mathrm{N}]^2[\mathrm{He}] \tag{24}$$

Substitution of $d[\mathrm{N}]/dt$ from Eq. (24) into Eq. (23), one obtains

$$[\mathrm{N}(t)] = \frac{-d\ln I_{N_2(B)}(t)/dt}{4k_1(v', \mathrm{He})[\mathrm{He}]}. \tag{25}$$

Once the intensity of the emission, $I_{N_2(B)}$, has been measured as a function of time, the density of N atoms at any time in the afterglow can be calculated from Eq. (25). However, if the rate constant of reaction (1) is not known, an additional experiment must be performed to obtain this parameter. In this case, one may use nitric oxide titration to find the concentration of N atoms at a given point in time in the afterglow, and then calculate $k_1(v', \text{He})$ from this value and the derivative of the $N_2(B)$ intensity.

A linear relationship between $1/(d\ln(I_{N_2(B)}(t))/dt)$ and t can be obtained by solving Eq. (24),

$$\frac{1}{[\text{N}(t)]} = \frac{1}{[\text{N}(t_0)]} + 2k_1(v', \text{He})[\text{He}](t - t_0) \tag{26}$$

Then substituting the nitrogen-atom concentration from Eq. (25) into Eq. (26) produces the following relationship:

$$\frac{1}{d\ln I_{N_2(B)}(t)/dt} = -\frac{1}{4k_1(v', \text{He})[\text{He}][\text{N}(t_0)]} - \frac{t}{2} \tag{27}$$

Equation (27) indicates that a plot of $1/(d\ln(I_{N_2(B)}(t))/dt)$ vs. t should be linear with a slope of 0.5.

This method is valid in the late afterglow where the emission of $N_2(B)$ is predominantly created from the N + N + He recombination reaction. In the early afterglow, the emission intensity of $N_2(B)$ is derived from two sources, (1) N atom recombination and (2) reactions from other active species expressed below as f. Equation (21) then becomes

$$I_{N_2(B)} = \alpha[\text{N}]^2 + f \tag{28}$$

As a result, the relationship of $1/(d\ln(I_{N_2(B)}(t))/dt)$ vs. t is not linear in this region. Nevertheless, the mechanism for N-atom decay is the same throughout the afterglow.[25] Therefore, one can use the linear relationship between $1/(d\ln(I_{N_2(B)}(t))/dt)$ and time to extrapolate to the edge of the discharge and obtain the initial density of nitrogen atoms.

3. EXPERIMENTAL METHODS

The atmospheric pressure plasma used in these experiments has been described previously.[14] A schematic of the source is shown in Fig. 1. It consisted of two parallel-plate electrodes separated by a gap 1.6 mm across. The upper aluminum electrode was 10.2 cm wide by 7.9 cm long and was driven by rf power at 13.56 MHz, while the lower stainless steel electrode was 10.2 cm wide by 20.4 cm long and was grounded. Just downstream of the upper electrode was a 1.3 cm × 10.2 cm wide Teflon plate, followed by

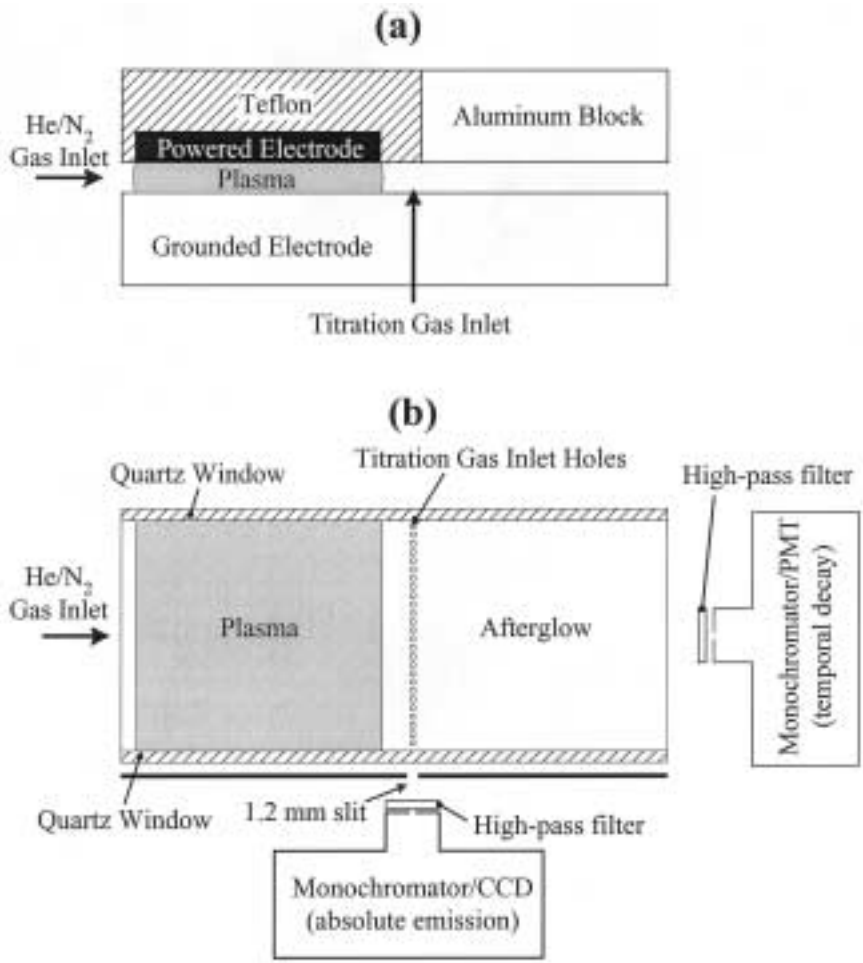

Fig. 1. **(a)** Side view of the plasma source. **(b)** Top view of the interior of the plasma source.

an aluminum plate, $10.2 \times 10.2\,\text{cm}^2$. These parts were mounted to provide a uniform duct 1.6 mm in height through the entire length of the device to avoid any disturbance of the gas flow in the afterglow region. The sides of the duct parallel to the flow direction were sealed with quartz windows so that spectroscopic measurements of the gas could be made. The neutral gas temperature was measured by two methods, (1) by utilizing an ungrounded thermocouple, 0.8 mm in diameter and (2) by calculating the rotational temperature of the (3, 0) band of the N_2 first positive emission spectrum.[33]

The plasma was operated at 200 W of rf power, a total flow rate of 30.4 L/min, 745 Torr of helium, and 10 Torr of nitrogen. Alternatively, the plasma could be operated with argon instead of helium when an RF frequency of 27.12 MHz was used. The flow rates produced a linear velocity of 3.7 m/s. This corresponded to a Reynold's number of 50, which was well within the laminar-flow regime. The helium and nitrogen were both of ultra-high purity (99.999%), while the nitric oxide was of commercial purity (99%). The helium and nitrogen were passed through an oxygen absorbing purifier (Matheson Gas Products, 6413) to further reduce oxygen and water impurities.

To determine the concentration of nitrogen atoms by the absolute emission of the $N_2(B, v')$ species, the rf power was applied continuously at 200 W. As shown in Fig. 1b, measurements were taken perpendicular to the gas flow direction. A concentration profile was obtained by translating the source in front of the detection system. The light emission was collected through a slit, 1.2 mm wide, a 550 nm high-wavelength-pass filter, and directly onto the entrance slit, 0.1 mm wide, of a monochromator (Instruments S.A., Triax 320). The emission spectra were measured by a liquid nitrogen cooled CCD detector (Instruments S.A., CCD-3000). Under these conditions, the spectral resolution was 0.2 nm. The absolute emission intensity as a function of wavelength was carefully calibrated by a quartz halogen standard tungsten lamp (Oriel, 63976). The detailed calibration procedure has been described previously.[14]

To determine the temporal decay of the $N_2(B, v')$ emission, the rf power was run in the pulsed mode. The rf power was applied for a 50 ms pulse at 200 W with a 20% duty cycle. This duty cycle was selected so that the decay of the rf power did not effect the results of the experiment. The delay time recorded in these experiments refers to the time elapsed after the rf power had been turned off in each pulse cycle. The temporal profiles of the emission were measured with a photo-multiplier tube (PMT) (Hamamatsu, R928P) attached to the monochromator. For these experiments, the plasma source was rotated so that the plasma emission could be observed parallel to the flow direction as shown in Fig. 1b. A 550 nm high-wavelength-pass filter was mounted in front of the monochromator entrance slit. The response time for this detection system was 3.0 μs.

For the nitric oxide titration experiments, an NO/He mixture was fed to the system through an array of 62 holes, each 0.8 mm in diameter, across the width of the lower grounded electrode. This array was located 1.2 cm downstream of the edge of the plasma discharge. The light emission was measured at the point where the nitric oxide and plasma effluent mix. To avoid overlap with the molecular nitrogen emission, the NO(B) emission was measured at 320 and 304 nm. No light filters were used for these

measurements. The presence of ground-state nitrogen dioxide was measured by an infrared spectrometer (BioRad FTS-7 equipped with an MCT detector). The NO_2 was monitored at 1627 cm^{-1} with an instrument resolution of 4 cm^{-1}.

4. RESULTS AND DISCUSSION

4.1. NO Titration

Shown in Fig. 2 is the NO(B) and NO_2 intensities as a function of the nitric oxide concentration in the afterglow. The plasma was operated at 200 W, 10 Torr N_2 and 745 Torr He. Since the intensities of NO(B) and NO_2 were not calibrated to give an absolute concentration, the intensities of the two curves were scaled to better view the results of the titration. The titration point occurs between the inflection points of the two curves (shaded region in the figure). By this technique, the nitrogen atom concentration was found to be $2.0 \pm 1.0 \times 10^{15}$ cm^{-3} at 1.2 cm downstream from the discharge edge. The gas temperature at this point was found to be 350 K

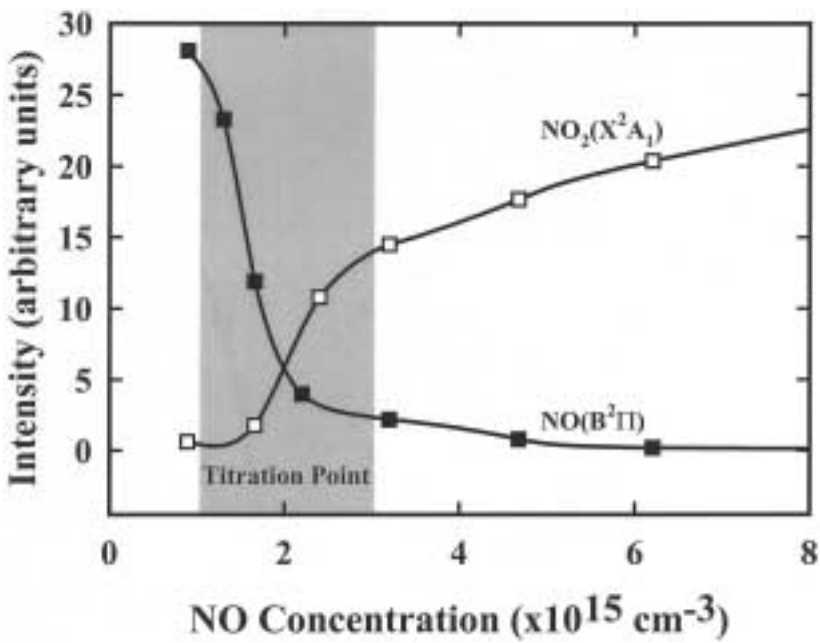

Fig. 2. The dependence of the NO(B) and NO_2 intensities on the nitric oxide concentration injected into the afterglow.

from the thermocouple and the rotational temperature of the first positive emission. These two measurements agreed to within 35 K.

4.2. Absolute Emission Intensity of $N_2(B, v')$

The reaction rate constant, $k_1(v', M)$, for the recombination of nitrogen atoms can be calculated from Eq. (19) for each vibrational level. To apply this equation, an N-atom density of $2.0 \times 10^{15}\,cm^{-3}$ was used as determined by NO titration. In addition, the $N_2(B, v')$ concentrations were calculated from the absolute emission calibration with the tungsten standard lamp, and $k_2(v', v'')$ and $k_3(v', N_2)$ were obtained from the literature.[31,32] The values for $k_3(v', He)$ were only available for $v' = 9$, 10, 11, 12,[24] so we assumed $k_3(v', He) = k_3(v', Ar)$ for $v' = 0$ to 8.[29] With these values, $k_1(v', He)$ was calculated for each vibrational level, and the results are shown in Fig. 3. The relative values of $k_1(v', He)$ for the different vibrational levels in Fig. 3 are similar to the results of Callede *et al.*,[30] in which the process gas was composed of argon with 4.0% nitrogen. For both cases, the

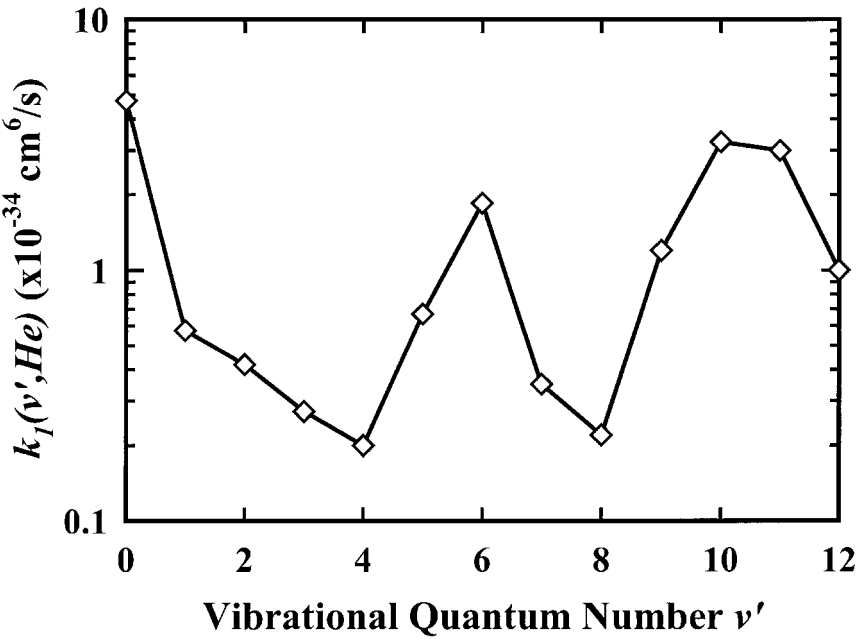

Fig. 3. The N + N + He recombination rate constant, $k_1(v', He)$, for vibrational levels 0 through 12. The uncertainty is estimated to be 57% of the reported value.

smallest rate constants occur at $v' = 4$ and 8. The total reaction rate $\sum_{v'} k_1(v', \text{He}) = 1.8 \pm 1.0 \times 10^{-33}\ \text{cm}^6/\text{s}$.

4.3. $N_2(B)$ Temporal Decay

The temporal decay curves of $N_2(B,\ v')$ for vibrational levels $v' = 2, 7$, and 11, measured at 773 nm, 653 nm and 579 nm, are shown in Fig. 4. The intensities of the temporal profiles were obtained directly from the photomultiplier tube. At small delay times, the three curves do not decrease at the same rate. The difference can be attributed to the presence of several mechanisms for creating $N_2(B)$ in the early afterglow, as discussed above. However, beyond a delay time of approximately 2 ms the three curves are parallel to each other indicating that reaction (1) dominates.

Shown in Fig. 5 is a plot of the inverse of the time derivative of the $N_2(B, 7)$ emission intensity, $1/(d\ln(I_{N_2(B)}(t))/dt)$, vs. time. The dashed line represents the "best fit" to the data from 2 to 12 ms. It exhibits a slope of 0.49 ± 0.03 and a y-intercept of 1.15 ± 0.05, demonstrating excellent agreement with the theory, i.e., Eq. (27). The method is valid for the region in which the plot of $1/(d\ln(I_{N_2(B)}(t))/dt)$ vs. t is linear, i.e., for ≥ 2 ms. For $t < 2$ ms, the experiment over-predicts the N-atom concentration because the

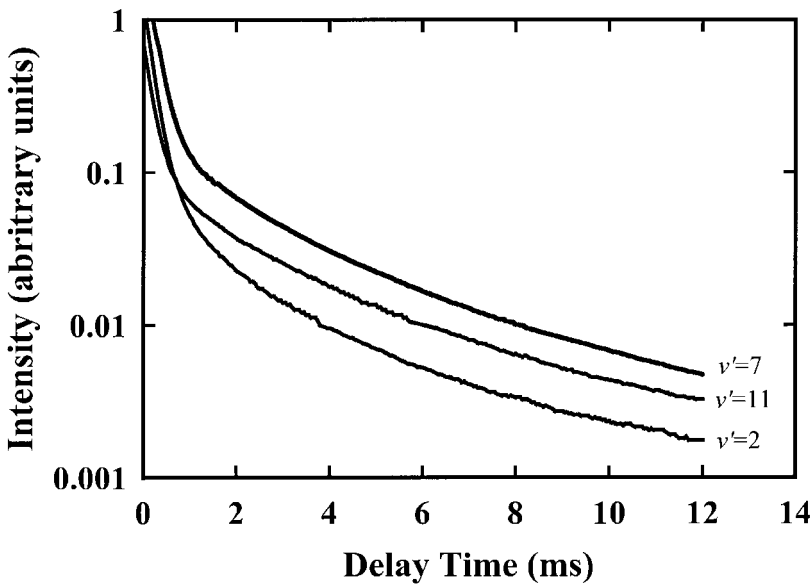

Fig. 4. The temporal decay of the $N_2(B, v')$ emission intensities for three vibrational states.

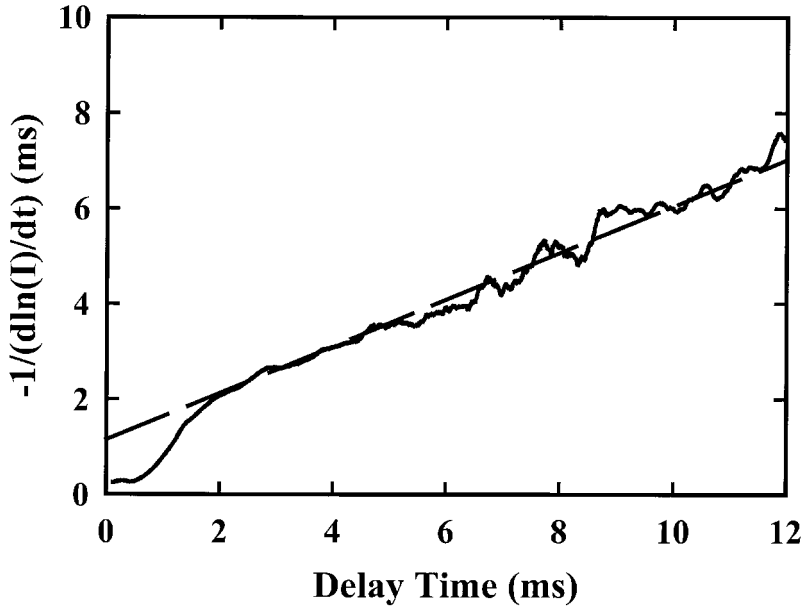

Fig. 5. The dependence of $1/(d\ln(I_{N_2(B)}(t))/dt)$ on time elapsed after the discharge is switched to the off state for $v' = 7$.

$N_2(B)$ at this stage is also created from other reactions, such as Eqs. (5) and (6).

From Eq. (25), the total recombination reaction constant, k_1, or the N-atom density can be calculated if the other is known. The titration was performed at a distance of 1.2 cm downstream from the discharge edge, which is equivalent to a 3.26 ms delay time. Using Eq. (25) and a N-atom density of $2.0 \pm 1.0 \times 10^{15}\,\mathrm{cm}^{-3}$, we obtained $k_1 = 2.2^{+2.2}_{-0.7} \times 10^{-33}\,\mathrm{cm}^6/\mathrm{s}$. This value is the same within experimental error as $\sum_{v'} k_1(v', \mathrm{He})$ calculated from the $N_2(B, v')$ absolute emission intensity. Using an activation energy of –0.975 kcal/mol for the N + N + M recombination reaction,[22] one obtains a value for k_1 at 298 K of $2.8^{+2.8}_{-0.9} \times 10^{-33}\,\mathrm{cm}^6/\mathrm{s}$. This agrees well with rate constants of 3.8 and $5.3 \times 10^{-33}\,\mathrm{cm}^6/\mathrm{s}$ at 298 K reported in the literature.[22,23]

4.4. Comparison of the Three Methods

The three methods of measuring the density of nitrogen atoms are compared in Fig. 6. In this figure, the filled circle indicates the value determined by NO titration, the diamonds represent the values obtained from the

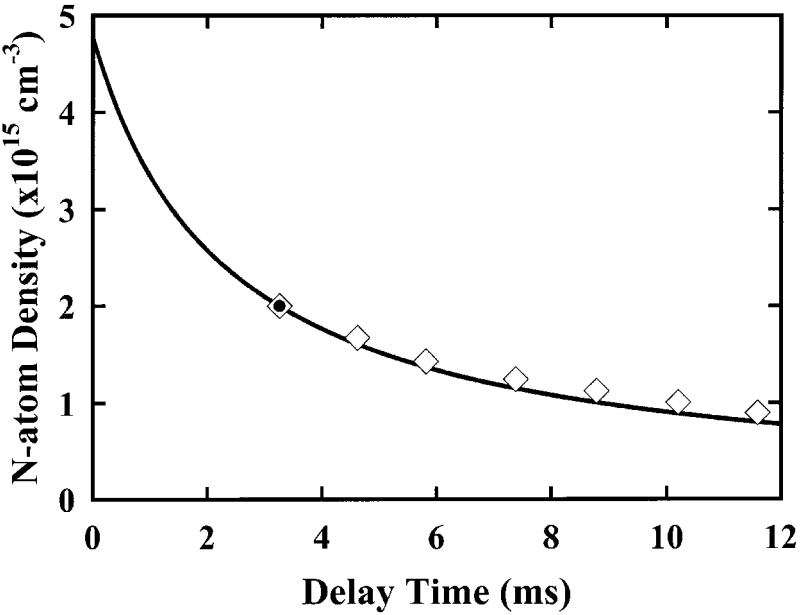

Fig. 6. Comparison of the N atom densities calculated by the three methods: NO titration (filled circle), absolute $N_2(B, v')$ calibrated emission (diamonds) and $N_2(B, v')$ temporal decay (solid curve).

$N_2(B, v')$ absolute emission, and the curve shows the N-atom concentration profile determined by the temporal decay of the $N_2(B, 7)$ emission intensity. The titration experiment was used to obtain the rate constant $k_1(v', \mathrm{He})$. Thus, the nitrogen atom concentrations obtained by all three methods will be the same at this point. The decay profiles of the second and third methods agree with each other.

Of the three methods, the titration is the most complicated since it requires the delivery of an accurate concentration of nitric oxide to a well-defined position in the afterglow. However, it is independent of the gas temperature and the third body species. On the other hand, the absolute emission of $N_2(B, v')$ is less complicated, and it does not disrupt the afterglow. Nevertheless, the need for an absolute intensity calibration limits its application. In addition, the calculations involved in this method require reaction rate constants that are sensitive to vibrational levels, temperature, and third body species. The method of measuring the temporal decay of $N_2(B, v')$ emission is the easiest to apply. Furthermore, the plot of $1/(d\ln(I_{N_2(B)}(t))/dt)$ vs. time can be extended back to the edge of the discharge to estimate the N-atom density in the early stages of the afterglow.

This is not possible with the other two methods. In order to apply this last technique, one needs to know $k_1(v', \text{He})$, which we have determined for reaction (1) in helium at atmospheric pressure (refer to Fig. 3).

To verify that our experiments were not effected by the presence of $N_2(A)$, the ratio of $[N_2(A)]/[N]$ was obtained at a distance of 1.2 cm downstream of the discharge edge. This ratio is evaluated by adding a relatively small amount of nitric oxide to the gas mixture. The NO is consumed by reaction with either N atoms, of $N_2(A)$ molecules, Eqs. (8) and (12), respectively, in Table II. In the former case, the final product is NO(B) via Eq. (9), whereas in the latter case, the product is NO(A). Applying the pseudo-steady-state approximation, $d[\text{NO}(B)]/dt = 0$, $d[\text{O}]/dt = 0$, and $d[\text{NO}(A)]/dt = 0$, one obtains

$$\frac{[\text{N}]}{[\text{N}_2(A)]} = \frac{k_{12}}{k_8}\frac{[\text{NO}(B)]}{[\text{NO}(A)]} \tag{29}$$

The NO(B) and NO(A) emissions were observed at 304 and 300 nm, respectively. Since these two peaks are separated by only 4 nm, we can assume that the response coefficients for the detection system are approximately the same. The Einstein coefficients for the NO(A) and NO(B) peaks are 8.8×10^4 and $8.9 \times 10^4\ \text{s}^{-1}$, respectively.[34,35] Adding this information to Eq. (29) we get

$$\frac{[\text{N}]}{[\text{N}_2(A)]} \cong 3\frac{I_{\text{NO}(B)}}{I_{\text{NO}(A)}} \tag{30}$$

where $I_{\text{NO}(B)}$ and $I_{\text{NO}(A)}$ represent the emission intensities of NO(B) and NO(A) at 304 nm and 300 nm, respectively.

In our titration experiments, the NO(A) peak could not be detected, which implies that the ratio of $I_{\text{NO}(B)}$ and $I_{\text{NO}(A)}$ must be larger than 100. This means that the nitrogen atom concentration must be about 300 times greater than the metastable nitrogen concentration at 1.2 cm downstream of the discharge edge. The three techniques discussed in this work were performed at or beyond this position. Thus we conclude that the $N_2(A)$ concentration did not effect any of the techniques used to determine the density of nitrogen atoms in the afterglow.

5. CONCLUSIONS

The nitrogen atom density in the afterglow of an N_2/He atmospheric pressure plasma has been determined by nitric oxide titration, by calibrating the $N_2(B, v')$ emission intensity and by measuring the decay of the $N_2(B)$ emission intensity while pulsing the plasma. The latter method is a new

convenient way to diagnose the density of nitrogen atoms throughout the entire afterglow. According to this method, the concentration of nitrogen atoms at the edge of the atmospheric pressure plasma discharge is $5.0 \pm 2 \times 10^{15}\,\mathrm{cm}^{-3}$ for 10 Torr N_2, 745 Torr He, and a power density of $15.5\,\mathrm{W/cm}^3$.

ACKNOWLEDGMENTS

This research was supported by grants from the UC SMART program and the National Science Foundation, Division of Chemical and Thermal Systems. The authors are grateful for their generous support.

REFERENCES

1. G. Lucovsky, H. Niimi, Y. Wu, C. R. Parker, and J. R. Hauser, *J. Vac. Sci. Technol. A* **16**, 1721 (1998).
2. J. A. Theil, S. V. Hattangady, and G. Lucovsky, *J. Vac. Sci. Technol. A* **10**, 719 (1992).
3. A. N. Wright and C. A. Winkler, "Active Nitrogen", Academic Press, New York (1968).
4. S. E. Alexandrov, M. L. Hitchman, and S. H. Shamlian, *J. Mater. Chem.* **5**, 457 (1995).
5. M. Gupta, V. K. Rathi, R. Thangaraj, O. P. Agnihotri, and K. S. Chari, *Thin Solid Films* **304**, 77 (1991).
6. C.-E. Moroosanu, *Thin Solid Films* **65**, 171 (1980).
7. B. F. Hanyaloglu and E. S. Aydil, *J. Vac. Sci. Technol. A* **16**, 2794 (1998).
8. J. Yota, J. Hander, and A. A. Saleh, *J. Vac. Sci. Technol. A* **18**, 372 (2000).
9. F. Delmotte, M. C. Hugon, B. Agius, and J. L. Courant, *J. Vac. Sci. Technol. A* **15**, 1919 (1997).
10. J. Y. Jeong, S. E. Babayan, V. J. Tu, J. Park, I. Henins, J. Verlarde, R. F. Hicks, and G. S. Selwyn, *Plasma Sources Sci. Technol.* **7**, 282 (1998).
11. J. Y. Jeong, S. E. Babayan, A. Schuetze, V. J. Tu, J. Park, I. Henins, G. S. Selwyn, and R. F. Hicks *J. Vac. Sci. Technol. A* **17**, 2581 (1999).
12. S. E. Babayan, J. Y. Jeong, V. J. Tu, J. Park, R. F. Hicks, and G. S. Selwyn, *Plasma Sources Sci. Technol.* **7**, 286 (1998).
13. A. Schütze, J. Y. Jeong, S. E. Babayan, J. Park, G. S. Selwyn, and R. F. Hicks, *IEEE Trans. Plasma Sci.* **26**, 1685 (1998).
14. J. Y. Jeong, J. Park, I. Henins, S. E. Babayan, V. J. Tu, G. S. Selwyn, G. Ding, and R. F. Hicks, *J. Phys. Chem.* **104**, 8027 (2000).
15. R. J. Strutt, *Proc. Roy. Soc.* **A85**, 219 (1911).
16. B. M. Anand, P. N. Kalia, and M. Ram, *Indian J. Phys.* **17**, 69 (1937).
17. T. Czerwiec, J. Gavillet, T. Belmonte, H. Michel, and A. Ricard, *J. Phys. III France* **6**, 1205 (1996).
18. R. A. Young and G. A. St. John, *J. Chem. Phys.* **48**, 895 (1968).
19. P. Merel, M. Tabbal, M. Chaker, M. Moisan, and A. Ricard, *Plasma Sources Sci. Technol.* **7**, 550 (1998).
20. M. F. Golde and B. A. Thrush, *Faraday Discuss. Chem. Soc.* **53**, 52 (1972).
21. A. M. Diamy, L. Hochard, J. C. Legrand, and A. Ricard, *Plasma Chem. Plasma Process.* **18**, 447 (1998).
22. I. M. Campbell and B. A. Thrush, *Proc. Roy. Soc.* (*London*) **A296**, 201 (1967).

23. R. A. Young and G. Black, *J. Chem. Phys.* **44**, 3741 (1965).
24. K. H. Becker, E. H. Fink, W. Groth, W. Jud, and D. Kley, *Faraday Discuss Chem. Soc.* **53**, 35 (1972).
25. J. F. Noxon, *J. Chem. Phys.* **36**, 926 (1962).
26. F. Kaufman, *J. Chem. Phys.* **28**, 992 (1958).
27. F. Kaufman and J. R. Kelso, *J. Chem. Phys.* **27**, 1209 (1957).
28. S. Bockel, A. M. Diamy, and A. Ricard, *Surg. Coat. Techn.* **74–75**, 474 (1995).
29. A. Ricard, J. Tetreault, and J. Hubert, *J. Phys. B* **24**, 1115 (1991).
30. G. Callede, J. Deschamps, J. L. Godart, and A. Ricard, *J. Phys. D: Appl. Phys.* **24**, 909 (1991).
31. F. R. Gilmore, R. R. Laher, and R. J. Espy, *J. Phys. Chem. Ref. Data* **21**, 1005 (1992).
32. L. G. Piper, *J. Chem. Phys.* **88**, 6911 (1988).
33. M. Simek and S. D. Benedictis, *Plasma Chem. Plasma Process.* **15**, 451 (1995).
34. L. G. Piper and L. M. Cowles, *J. Chem. Phys.* **85**, 2419 (1986).
35. L. G. Piper, T. R. Tucker, and W. P. Cummings, *J. Chem. Phys.* **94**, 7667 (1991).